

1 **Model selection: Using information measures from ordinal symbolic**
2 **analysis to select model sub-grid scale parameterizations**

3 Manuel Pulido *

4 *Department of Physics, FaCENA,*

5 *Universidad Nacional del Nordeste (UNNE) and CONICET,*

6 *Corrientes, Argentina.*

7 Osvaldo A. Rosso ^{1,2,3}

8 ¹ *Instituto de Física, Universidade Federal de Alagoas (UFAL)*

9 *Maceió, AL, Brazil.*

10 ² *Instituto Tecnológico de Buenos Aires (ITBA) and CONICET,*

11 *Ciudad Autónoma de Buenos Aires, Argentina.*

12 ³ *Complex Systems Group, Facultad de Ingeniería y Ciencias Aplicadas,*

13 *Universidad de los Andes,*

14 *Las Condes, Santiago, Chile.*

15 *Corresponding author address: Manuel Pulido, Department of Physics, FaCENA, Universidad

16 Nacional del Nordeste (UNNE), Av. Libertad 5400, Corrientes (3400), Argentina.

17 E-mail: pulido@exa.unne.edu.ar

ABSTRACT

18 The use of information measures for model selection in geophysical models
19 with subgrid parameterizations is examined. Although the resolved dynamical
20 equations of atmospheric or oceanic global numerical models are well established,
21 the development and evaluation of parameterizations that represent subgrid-scale
22 effects pose a big challenge. For climate studies, the parameters or parameterizations
23 are usually selected according to a root-mean-square error criterion, that measures
24 the differences between the model state evolution and observations along the trajectory.
25 However, inaccurate initial conditions and systematic model errors contaminate
26 root-mean-square error measures. In this work, information theory quantifiers, in
27 particular Shannon entropy, statistical complexity and Jensen-Shannon divergence,
28 are evaluated as measures of the model dynamics. An ordinal analysis is conducted
29 using the Bandt-Pompe symbolic data reduction in the signals. The proposed ordinal
30 information measures are examined in the two-scale Lorenz'96 system. By comparing
31 the two-scale Lorenz'96 system signals with a one-scale Lorenz'96 system with
32 deterministic and stochastic parameterizations, we show that information measures
33 are able to select the correct model and to distinguish the parameterizations
34 including the degree of stochasticity that results in the closest model dynamics
35 to the two-scale Lorenz'96 system.

37 **1. Introduction**

38 The numerical models for climate predictions and weather forecasts involve a set of dynamical
39 equations which represents the atmospheric or oceanic motions on a grid. Coupled to the re-
40 solved dynamical equations of the models, there is a set of parameterizations which represents the
41 subgrid-scale physical processes. The model parameterizations are responsible for a large fraction
42 of model error and thus for the resultant uncertainty associated to climate predictions (see e.g.
43 Stainforth et al. 2005). One major challenge in model development is to decrease model error
44 by recovering aspects of the natural system evolution represented by the parameterizations in the
45 model. However, the actual dynamics of the system is unknown; limited and sparse observations
46 with associated measurement errors is the only source of information of the natural system evo-
47 lution. The usual procedure for parameterization development and also for inferring unknown
48 parameters is to tune the parameterization or the parameters in order to decrease root-mean-square
49 errors between the model integrations and the observations starting from initial conditions that
50 are close to the natural system state at a given time. For short times, the model state is close to
51 the natural system state, so that model sensitivity should follow natural system sensitivity (Pulido
52 2014). However, systematic model errors drift the model state from the natural system trajectory
53 for long times (from 5-days); therefore the model and the natural system differ substantially. In
54 this context, observed natural system sensitivity is not useful to constrain model sensitivity, and
55 root-mean-square errors give limited information for model improvement.

56 Data assimilation techniques have been proposed as a method for estimating model parameters
57 (Ruiz et al. 2013a; Aksoy 2015) and for model development (Pulido et al. 2016; Lang et al. 2016).
58 In a data assimilation system, the model state is recursively pushed towards the observations at
59 the analysis times so that one expects that model sensitivity can be constrained from the observed

60 natural system sensitivity. Under the presence of multiple sources of model errors in a realistic
61 scenario, the estimation of model parameters with data assimilation techniques compensates not
62 only model errors due to the physical process represented in that parameterization but also other
63 sources of model errors. For instance, Ruiz and Pulido (2015) show that estimating the parameters
64 associated with moist processes in an atmospheric general circulation model compensates not only
65 errors from convection but also errors produced by an incorrect representation of boundary layer
66 dynamics. Therefore, the estimated parameters are optimal for that particular combination of
67 model errors and for that particular point of the model state. In other situations, that estimated set
68 of parameters will not represent the natural system sensitivity.

69 Klinker and Sardeshmukh (1992) examined the initial tendency errors, the differences between
70 model sensitivity and observed sensitivity during the first time step from the initial conditions.
71 Rodwell and Palmer (2007) show that systematic initial tendency errors can be useful to assess
72 climate models. Errors from different sources should be decoupled at initial times and they should
73 be localized close to the source locations. In a multi-scale system, the errors that dominate at initial
74 times are produced by fast processes. The model sensitivity feedback interactions associated with
75 slow processes are expected to be weak compared with fast processes so that they will not be easily
76 captured by initial tendency errors (Rodwell and Palmer 2007).

77 The predictability of a dynamical system is quantified by the growth rate of errors as the system
78 evolves. For chaotic systems, a small error in the initial conditions grows as the prediction range
79 increases. The average long-term exponential separation between two trajectories which initially
80 differ by an infinitesimal distance is given by the leading Lyapunov exponent. If the leading Lyapunov
81 exponent is positive, the system is chaotic — errors grow with time. The leading Lyapunov
82 exponent is a possible measure to quantify the predictability of the dynamical system. There is a
83 strong relation between the Shannon entropy and the Lyapunov exponents. For a dynamical sys-

84 tem which has a sufficiently smooth probability distribution the Pesin identity holds, the sum of
85 the positive Lyapunov exponents is equal to the Kolmogorov-Sinai entropy (Pesin 1977; Eckmann
86 and Ruelle 1985). In this way, the permutation Shannon entropy can be considered as an upper
87 bound of the Lyapunov exponents (e.g. Bandt and Pompe 2002). Therefore, entropy is also a
88 useful quantity to characterize the predictability in the climate system.

89 Leung and North (1990) introduce Shannon entropy as a measure of the uncertainty in a climate
90 signal. They examine the similarities between a climate and a communication system. A state
91 in the climate system with large entropy would be unpredictable. There are many possible states
92 that are equally probable. Majda and Gershgoring (2011) propose to use information theory for
93 measuring model fidelity and sensitivity. They use the relative entropy to measure the distance
94 between the probability distribution functions (PDFs) of the natural system and of the numerical
95 model, assuming that both PDFs are Gaussian. Tirabassi and Massoller (2016) use symbolic time-
96 series analysis and mutual lag between time series at different grid points to identify communities
97 in climate data, i.e. sets of nodes densely interconnected in the network.

98 In the present work, we examine information theory measures as a tool to evaluate numeri-
99 cal models. We extend the concepts introduced by Majda and Gershgoring (2011) to the use of
100 Jensen–Shannon divergence (Grosse et al. 2002) computed with the ordinal symbolic PDFs. This
101 ordinal analysis is conducted using the Bandt and Pompe (2002) symbolic data reduction in the
102 signals, in particular, to determine the corresponding ordinal-based quantifiers, such as normalized
103 Shannon entropy and statistical complexity. They can be used to distinguish different dynamical
104 regimes and to discriminate clearly chaotic from stochastic signals (Rosso et al. 2007, 2012a,b).
105 By comparing information measures from time series of variables of a set of imperfect models
106 with information measures from observed time series, our aim is to find the imperfect numerical
107 model that is closest to the information measures of the natural system.

108 Information measures of the two-scale Lorenz'96 system (Lorenz 1996) are evaluated using
109 ordinal symbolic analysis as a function of the “physical” parameters of the system: the constant
110 forcing and the interaction coefficient between the slow and fast dynamics. This two-scale system
111 is then considered as the natural system evolution, while the numerical imperfect model is the
112 one-scale Lorenz'96 (Lorenz 1996). We assume the small-scale processes cannot be represented
113 explicitly in this imperfect model, so that the effects of small-scale processes are parameterized
114 as a polynomial function which depends on large-scale variables. The information measures from
115 ordinal symbolic analysis are used to find the most suitable parameterization of the small-scale
116 processes. The information measures of the imperfect model should be as close as possible to
117 the information measure of the “natural system”, the two-scale Lorenz'96 system. We evaluate
118 whether the measures are suitable for parameter selection, this is, whether parameter changes have
119 enough sensitivity in the information measures, so that the optimal parameters could be properly
120 inferred from information measures.

121 Physical parameterizations in atmospheric or oceanic numerical models represent the subgrid-
122 scale physical processes, through functional dependences with the resolved variables. These re-
123 solved variables, that the parameterizations depend on, are slow large-scale variables; hence in
124 general the models lack from small-scale variability. Palmer (2001) suggested the use of stochas-
125 tic parameterizations to account for this lack of variability in the models. There are several works
126 in the last decade that show that both weather forecasts and climate predictions appear to benefit
127 from stochastic parameterizations. For instance, the ensemble prediction system of the European
128 Center for Medium-range Weather Forecasts (ECMWF) uses a stochastic kinetic backscatter algo-
129 rithm to improve the skill of ensemble forecasting (Shutts 2005). Convection processes have also
130 been proposed to be represented through stochastic parameterizations (Christensen et al. 2015).
131 Some climate features, such as the quasi-biennial oscillation, are better represented in models with

132 stochastic parameterizations (Piani et al. 2004; Lott et al. 2012). Wilks (2005) showed that includ-
133 ing a stochastic parameterization in the Lorenz’96 system produces improvements compared to
134 deterministic parameterizations of both the model climatology and ensemble forecast verification
135 measures. Here, we evaluate whether the use of information measures is sensitive to stochastic
136 parameterizations and whether some of the noise variance parameters of stochastic parameteriza-
137 tions may be constrained by trying to reproduce with the model the information measures from
138 the observed time series.

139 **2. Information measures for characterizing model dynamics**

140 Chaotic dynamical systems are sensitive to initial conditions. These manifest instability every-
141 where in the phase space and lead to non-periodic motion, i.e. chaotic time series (Abarbanel
142 1996). They are unpredictable in the long term despite the deterministic character of the temporal
143 trajectory. In a system undergoing chaotic motion, two neighboring points in the phase space move
144 away exponentially. Let $\mathbf{x}_1(t)$ and $\mathbf{x}_2(t)$ be two such points, located within a ball of radius R at time
145 t . Further, assume that these two points cannot be resolved within the ball due to observational
146 error. At some later time t' the distance between the points will typically grow to

$$|\mathbf{x}_1(t') - \mathbf{x}_2(t')| \approx |\mathbf{x}_1(t) - \mathbf{x}_2(t)| \exp(\Lambda |t' - t|), \quad (1)$$

147 with $\Lambda > 0$ for chaotic dynamics, being Λ the leading Lyapunov exponent. When this distance at
148 time t' exceeds R , the points become observationally distinguishable. This implies that instability
149 reveals some information about the phase-space population that was not available at earlier times
150 (Abarbanel 1996). Thus, under the above considerations chaos can be thought as an *information*
151 *source*.

152 The information content of a system is typically evaluated via a PDF, P , describing the charac-
153 teristic behavior of some measurable or observable quantity, generally a time series $\mathcal{X}(t)$. Quan-
154 tifying the information content of a given observable quantity is therefore largely equivalent to
155 characterizing its probability distribution. This is often done with the wide family of measures
156 called information theory quantifiers (Gray 1990). We can define information theory quantifiers as
157 measures able to characterize relevant properties of the PDF associated with the time series which
158 can be generated from observations of a dynamical system or from model integrations.

159 *a. Ordinal symbolic analysis*

160 The evaluation of quantifiers derived from information theory, like Shannon entropy and sta-
161 tistical complexity, supposes some prior knowledge about the system; specifically, a probability
162 distribution associated to the time series under analysis should be provided beforehand. Although
163 for a physical quantum system, the concept of probability is uniquely defined; there are several
164 ways to define a probability distribution for a dynamical system. The traditional is the histogram,
165 the state space is partitioned into bins and by counting the number of times N_i that the trajectories
166 of an ensemble pass through the i -bin at a given time, the probability is, in this way, defined as
167 $p_i = N_i/N$, where N is the total number of trajectories. This symbolic sequence can be regarded
168 to as a non causal coarse-grained description of the time series under consideration.

169 An alternative definition is given with time sequences. Suppose we use a sequence of L time
170 steps and we label the bins, then in L time steps the trajectory passes through L bins, and we
171 can form a *symbolic sequence* of length L . In the symbolic sequence, each symbol from a finite
172 alphabet represents a bin, and the pattern is formed by the sequences of bins, which visits the
173 trajectory in the L time steps. Counting the occurrence of each pattern, over the total number of

174 sequences we determine the probability distribution. If we diminish the size of the bins, in the
 175 limit we can derive from this probability the Kolmogorov-Sinai entropy (Schuster and Just 2006).

176 For some dynamical systems, the information measures determined from bin-symbolic analysis
 177 are sensitive to the way the bins are generated (Bollt et al. 2000). Bandt and Pompe (2002) in-
 178 troduced a simple and robust symbolic methodology that takes into account time causality of the
 179 time series—a causal coarse-grained methodology—by comparing neighboring values in a time
 180 series. In this work, we refer as ordinal symbolic analysis to the Bandt and Pompe methodology.
 181 The symbolic data are: (i) created by ranking the values of the series; and (ii) defined by reorder-
 182 ing the embedded data in ascending order, which is equivalent to a phase-space reconstruction
 183 with embedding dimension (pattern length) D . In this way, the diversity of the ordering symbols
 184 (patterns) derived from a scalar time series is quantified.

185 The appropriated symbolic sequence arises naturally from the time series, and no system-based
 186 assumptions are needed in Bandt and Pompe methodology. In fact, the necessary “partitions” are
 187 devised by comparing the order of neighboring relative values rather than by apportioning ampli-
 188 tudes according to different levels. This technique, as opposed to most of those in current practice,
 189 takes into account the temporal structure of the time series generated by the physical process under
 190 consideration. As such, it allows us to uncover important details concerning the ordinal structure
 191 of the time series (Rosso et al. 2007) and can also yield information about temporal correlation
 192 (Rosso and Masoller 2009a,b).

193 The “ordinal patterns” of order (length) D in the Bandt and Pompe methodology are generated
 194 by

$$(s) \mapsto (x_{s-(D-1)}, x_{s-(D-2)}, \dots, x_{s-1}, x_s) , \quad (2)$$

195 which assigns to each time s the D -dimensional vector of values at times $s - (D - 1), \dots, s - 1, s$.

196 By “ordinal pattern” related to the time (s), we mean the permutation $\pi = (r_0, r_1, \dots, r_{D-1})$ of

197 $[0, 1, \dots, D-1]$ defined by

$$x_{s-r_{D-1}} \leq x_{s-r_{D-2}} \leq \dots \leq x_{s-r_1} \leq x_{s-r_0}. \quad (3)$$

198 In this way the vector defined by (2) is converted into a unique symbol π . We set $r_i < r_{i-1}$ if
 199 $x_{s-r_i} = x_{s-r_{i-1}}$ for uniqueness, although ties in samples from continuous distributions have null
 200 probability.

201 Then, the occurrence of each symbolic pattern is counted in the whole time series. The prob-
 202 ability of each symbol, π_i , is the number of occurrences of the pattern over the total number
 203 of analyzed sequences in the time series. The Bandt and Pompe PDF (BP-PDF) is given by
 204 $P = \{p(\pi_i), i = 1, \dots, D!\}$, with

$$p(\pi_i) = \frac{\#\{s | s \leq M - (D-1); (s) \text{ is of type } \pi_i\}}{M - (D-1)}, \quad (4)$$

205 where # denotes cardinality and M is the time series length.

206 In order to illustrate ordinal symbolic analysis, let us consider a simple example: a time se-
 207 ries with seven ($M = 7$) values $\mathcal{X} = \{4, 7, 9, 10, 6, 11, 3\}$ and compute the BP-PDF for $D = 3$.
 208 In this case, the state space is divided into $3!$ partitions so that 6 mutually exclusive permuta-
 209 tion symbols are considered. The triplets $(4, 7, 9)$ and $(7, 9, 10)$ represent the permutation pattern
 210 $\{012\}$, since they are in increasing order. On the other hand, $(9, 10, 6)$ and $(6, 11, 3)$ correspond
 211 to the permutation pattern $\{201\}$ since $x_{t+2} < x_t < x_{t+1}$, while $(10, 6, 11)$ has the permutation
 212 pattern $\{102\}$ with $x_{t+1} < x_t < x_{t+2}$. Then, the associated probabilities to the 6 patterns are:
 213 $p(\{012\}) = p(\{201\}) = 2/5$; $p(\{102\}) = 1/5$; $p(\{021\}) = p(\{120\}) = p(\{210\}) = 0$.

214 The existence of an attractor in the D -dimensional phase space is not required in the ordinal
 215 symbolic analysis. The only condition for the applicability of the method is a very weak stationary
 216 assumption. For $k \leq D$, the probability for $x_t \leq x_{t+k}$ should not depend on t .

217 *b. Entropy, statistical complexity and Jensen-Shannon divergence*

218 Entropy is a basic quantity with multiple field-specific interpretations. For instance, it has been
219 associated with disorder, state-space volume, and lack of information (Brissaud 2005). When
220 dealing with information content, the Shannon entropy is often considered as the foundational
221 and most natural one (Shannon 1948; Shannon and Weaver 1949). It is a positive quantity that
222 increases with increasing uncertainty and is additive for independent components of a system.
223 From a mathematical point of view, Shannon entropy is the only information measure that satisfies
224 the Kinchin axioms (Khinchin 1957).

225 Let $P = \{p_i; i = 1, \dots, N\}$ with $\sum_{i=1}^N p_i = 1$, be a discrete probability distribution, with N the
226 number of possible states of the system under study. The “Shannon” logarithmic information
227 measure is defined by

$$S[P] = - \sum_{i=1}^N p_i \ln(p_i) . \quad (5)$$

228 This can be regarded to as a measure of the uncertainty (lack of information) associated to the
229 physical process described by P . For instance, if $S[P] = S_{\min} = 0$, we are in a position to predict
230 with complete certainty which of the possible outcomes i , whose probabilities are given by p_i ,
231 will actually take place. Our knowledge of the underlying process described by the probability
232 distribution is maximal in this instance. In contrast, our knowledge is minimal for a uniform
233 distribution $P_e \equiv \{p_i = 1/N, i = 1, \dots, N\}$ since every outcome exhibits the same probability of
234 occurrence. Thus, the uncertainty is maximal, i.e., $S[P_e] = S_{\max} = \ln N$. In the discrete case, we
235 define a “normalized” Shannon entropy, $0 \leq \mathcal{H} \leq 1$, as

$$\mathcal{H}[P] = S[P]/S_{\max} . \quad (6)$$

236 Statistical complexity is often characterized by a complicated dynamics generated from rela-
237 tively simple systems. Obviously, if the system itself is already involved enough and is constituted

238 by many different parts, it may clearly support a rather intricate dynamics, but perhaps without
 239 the emergence of typical characteristic patterns (Kantz et al. 1998). Therefore, a complex system
 240 does not necessarily generate a complex output. Statistical complexity is therefore related to struc-
 241 tures hidden in the dynamics, emerging from a system which itself can be much simpler than the
 242 dynamics it generates (Kantz et al. 1998).

243 We follow the original idea for statistical complexity introduced by López-Ruiz et al. (1995).
 244 A suitable complexity measure should vanish both for completely ordered and for completely
 245 random systems and it cannot only rely on the concept of information (which are maximal and
 246 minimal for the above mentioned systems). It can be defined as the product of a measure of
 247 information and a measure of disequilibrium, i.e. some kind of distance from the equiprobable
 248 distribution of the accessible states of a system (López-Ruiz et al. 1995; Lamberti et al. 2004).

249 The statistical complexity measure to be used here (Lamberti et al. 2004; Rosso et al. 2007) is
 250 defined through the functional product form

$$\mathcal{C}[P] = Q_{JS}[P, P_e] \cdot \mathcal{H}[P] \quad (7)$$

251 of the normalized Shannon entropy \mathcal{H} , see (6), and the disequilibrium Q_{JS} . It is defined in terms
 252 of the Jensen-Shannon divergence $D_{JS}[P, P_e]$,

$$Q_{JS}[P, P_e] = Q_0 \cdot D_{JS}[P, P_e] = Q_0 \cdot \{S[(P+P_e)/2] - S[P]/2 - S[P_e]/2\}, \quad (8)$$

253 where Q_0 is equal to the inverse of the maximum of $D_{JS}[P, P_e]$ which is obtained when one of the
 254 components of P is one and the remaining are zero. Therefore, the disequilibrium Q_{JS} measures
 255 the normalized distance of the probability distribution of the system under study P and the uniform
 256 distribution P_e which is the equilibrium PDF.

257 For a given value of \mathcal{H} , the range of possible \mathcal{C} values varies between a minimum \mathcal{C}_{min} and
 258 a maximum \mathcal{C}_{max} , restricting the possible values of the statistical complexity measure (Martín

et al. 2006). The planar representation entropy-complexity plane, $\mathcal{H} \times \mathcal{C}$, is an efficient tool to distinguish between the deterministic chaotic and stochastic nature of a time series since the permutation quantifiers have distinctive behaviors for different types of dynamics (Rosso et al. 2007). This tool has also been used for visualization and for a characterization of different dynamical regimes when the system parameters vary (Zanin et al. 2012).

Finally, we consider a measure for model evaluation against the observed time series. A measure of the distance between the probabilities from the model and observed time series. This concept has been used earlier by Majda and Gershgoring (2011) who called it model fidelity. They use the Kullback-Leibler relative entropy to measure the distance between the two probabilities. Arnold et al. (2013) evaluated the use of Hellinger distance and Kullback-Leibler distance in the Lorenz'96 system. The two measures gave similar performance. We use the Jensen-Shannon divergence to measure the distance between the probabilities to be coherent with the information theory quantifiers used in this work and because it is a symmetric positive-definite quantity. The square-root of the Jensen-Shannon divergence satisfies metric properties and triangle inequality (Lin 1991).

Assuming P_M and P_O are the corresponding BP-PDFs from the model time series and from the observed time series respectively, the Jensen-Shannon divergence is defined as a symmetric measure of the Kullback-Leibler divergence,

$$D_{JS}[P_M, P_O] = \sum \left[p_i^M \ln(p_i^M / p_i^O) + p_i^O \ln(p_i^O / p_i^M) \right] = \sum (p_i^M - p_i^O) \ln(p_i^M / p_i^O), \quad (9)$$

it vanishes when $p_i^M = p_i^O$ for all i . It can also be expressed in terms of the Shannon entropy (5):

$$D_{JS}[P_M, P_O] = S[(P_M + P_O)/2] - S[P_M]/2 - S[P_O]/2. \quad (10)$$

To evaluate (10), we determine the probability of the observed time series P_O and of the different model time series P_M using ordinal symbolic analysis. The Jensen-Shannon divergence is a measure of distance between two PDFs, P_M and P_O , so that a small Jensen-Shannon divergence

280 indicates a model PDF close to the observed PDF. The best model or the optimal parameters are
 281 the ones whose the time series gives the smallest Jensen-Shannon divergence.

282 3. Description of the numerical experiments

283 In the numerical experiments, we evaluate the potential of ordinal symbolic analysis to select
 284 subgrid-scale parameterizations using the integration of the two-scale Lorenz'96 system (Lorenz
 285 1996) as the natural system evolution. The equations of this system are given by a set of N
 286 equations of large-scale variables X_n ,

$$\frac{dX_n}{dt} + X_{n-1}(X_{n-2} - X_{n+1}) + X_n = F - \frac{hc}{b} \sum_{j=(M/N)(n-1)+1}^{nM/N} Y_j ; \quad (11)$$

287 where $n = 1, \dots, N$; and a set of M equations of small-scale variables Y_m , given by

$$\frac{dY_m}{dt} + c b Y_{m+1}(Y_{m+2} - Y_{m-1}) + c Y_m = \frac{hc}{b} X_{\text{int}[(m-1)/(M/N)]+1} ; \quad (12)$$

288 where $m = 1, \dots, M$. Note that both sets of equations (Eqs. (11) and (12)) are in a periodic domain,
 289 that is $X_0 = X_N$, $X_{-1} = X_{N-1}$ and $Y_0 = Y_M$, $Y_1 = Y_{M+1}$, $Y_2 = Y_{M+2}$.

290 Equations (11) and (12) are essentially the same but with different scales. They have coupling
 291 terms between them, the equations of small-scale variables, (12), are forced by the local (closest)
 292 large-scale variable. The equations of large-scale variables, (11), are forced by the external forcing
 293 F , and by the averaged small-scale variables which are located around the large-scale variable in
 294 consideration.

295 Lorenz (1996) suggested this simple model as a one-dimensional atmospheric model with two
 296 distinct time scales in a latitudinal circle with interactions between the two scales and he used
 297 it to illustrate atmospheric predictability issues. In the experiments, we use the standard set of
 298 constants: $N = 8$, $M = 256$, coupling constant $h = 1$, time-scale ratio $c = 10$, and spatial-scale

299 ratio $b = 10$ (unless stated otherwise). Note that setting $h = 0$ in (11), we recover the one-scale
 300 Lorenz'96 system.

301 In reality, the atmospheric numerical models cannot represent the small-scale variables associ-
 302 ated with convection processes, small-scale waves, etc., so that the effects of the small-scale vari-
 303 ables on the large-scale equations must be parameterized in the numerical models through forcing
 304 terms with functional dependencies of only the large-scale variables and a set of free parameters.
 305 Thus, the equations of the *imperfect model* are

$$\frac{dX_n^M}{dt} + X_{n-1}^M(X_{n-2}^M - X_{n+1}^M) + X_n^M = G_n(X_n^M, a_0, \dots, a_J); \quad (13)$$

306 where $n = 1, \dots, N$ and X_n^M represents the variables of the imperfect model. The function
 307 $G_n(X_n^M, a_0, \dots, a_J)$ is a parameterization of the small-scale processes and the forcing term, it seeks
 308 to mimic the right hand side term of (11). The a_j are free parameters.

309 Two representations of the forcing term are examined in this work: *a) a deterministic parame-*
 310 *terization* given by a polynomial function,

$$G_n(X_n^M, a_0, \dots, a_J) = \sum_{j=0}^J a_j \cdot (X_n^M)^j; \quad (14)$$

311 and *b) a stochastic parameterization* defined in Wilks (2005) by a polynomial function and a
 312 stochastic component given by realizations of a first-order autoregressive process

$$G_n(X_n^M, a_0, \dots, a_J, \sigma, \phi) = \sum_{j=0}^J a_j \cdot (X_n^M)^j + \eta_n(t); \quad (15)$$

313 where

$$\eta_n(t) = \phi \eta_n(t - \Delta t) + \sigma (1 - \phi^2)^{1/2} v_k(t), \quad (16)$$

314 ϕ is the autoregressive parameter, v_k is a realization of a normal distribution with zero mean and
 315 unit variance, and σ is the standard deviation of the process. Both ϕ and σ , apart from a_j , are free
 316 parameters.

317 The Lorenz'96 system was integrated using a Runge-Kutta of fourth order, with an integration
318 step of $\delta = 0.001$. In what follows the time resolution of the time series or the observational time
319 resolution is taken to be $\delta = 0.05$ (this corresponds to observations every 50 timesteps), which
320 considering the growth rates of the system, it represents 6 hours in the atmosphere and so it is
321 able to capture the instability growth (Lorenz 1996). To avoid spin-up behavior, the state is started
322 from a random initial condition and it is integrated by 10^5 observational times (this corresponds
323 to $5 \cdot 10^6$ time steps). The resulting state is used as the initial condition and it is integrated further
324 by $N_d = 10^5$ observational times (i.e. N_d is the time series length) which are used to compute the
325 information measures.

326 In order to evaluate the imperfect model, we use an “observed” time series of a single large-
327 scale variable from the natural system evolution, the two-scale Lorenz'96 system. That is, we
328 assume that the large-scale is the only information observed so that signals from a single large-
329 scale variable are used in the ordinal symbolic analysis. The small-scale dynamics is neither
330 modeled nor observed, except in the “true” state integration which is conducted with the two-scale
331 Lorenz'96 and considered as the natural system trajectory.

332 In all the experiments, we use the ordinal symbolic analysis to determine BP-PDFs associated
333 with the time series of the dynamical system and then the information quantifiers, normalized
334 Shannon entropy (6), statistical complexity (7) and Jensen-Shannon divergence (10), are com-
335 puted. The length of the pattern for the ordinal analysis is taken to be $D = 6$. This gives a total of
336 $D! = 6! = 720$ possible ordinal symbolic patterns, which clearly satisfy the condition $N_d \gg D!$ for
337 robust statistics (Rosso et al. 2007). The choice of the length of the pattern is a compromise deci-
338 sion, a longer D gives a more causal and higher resolution PDF, but it requires a longer time series
339 for accurate statistics. We took $D = 6$ as in Rosso et al. (2007); Serinaldi et al. (2014). However,

340 note that because of the short climate time series available, Tirabassi and Massoller (2016) used
341 $D = 3$ for monthly climate time series with meaningful results.

342 In a first set of experiments, we explore the two-scale Lorenz'96 system with the information
343 quantifiers: Shannon entropy (6) and statistical complexity (7). Different dynamical regimes are
344 uncovered as the forcing and the coupling coefficient are varied.

345 A second set of experiments focuses on model fidelity, in which we determine the BP-PDFs of
346 the observed time series P_O and of the modeled time series P_M , and so (10) is evaluated. Observed
347 and modeled time series are completely independent including the initial condition. They are
348 both assumed to be on the attractor of the dynamical system (after the spin-up integration). The
349 synthetic observed time series is in the second set of experiments generated with an integration of
350 the one-scale Lorenz '96 system and a set of prescribed parameter values. Then we can evaluate
351 the sensitivity of the information quantifiers to the model parameters for integration of the one-
352 scale Lorenz '96 system with different parameter values. In particular, we expect a minimum in the
353 Jensen-Shannon divergence when the model parameters are set at the “true” values (the ones used
354 to generate the observations). The evaluated parameterizations in this perfect model framework
355 are a deterministic parameterization, which consists of a quadratic polynomial function (14), and
356 a stochastic parameterization, which consists of a quadratic polynomial function and a first-order
357 autoregressive process (15).

358 To estimate the optimal parameter values, a genetic algorithm was implemented (Charbonneau
359 2002; Pulido et al. 2012). The genetic algorithm is an optimization Monte Carlo method inspired
360 in natural selection, in which a population of individuals is evolved and the fitness (cost function)
361 of each individual is evaluated. Processes of mutation, crossover and selection are considered
362 in the population evolution (see Charbonneau 2002 for further details on the algorithm). The
363 genetic algorithm is able to find the global minimum even in the presence of multiple local minima,

364 however it presents slow convergence (Pulido et al. 2012). Therefore, we opted for a combined
365 optimization method, the genetic algorithm is applied first, and then the newUOA optimization
366 (Powell 2006), using as initial guess parameters the ones estimated with the genetic algorithm. The
367 newUOA is an unconstrained minimization algorithm which does not require derivatives. Both, the
368 genetic algorithm and newUOA are suitable for control spaces of up to a few hundred dimensions.
369 The Jensen-Shannon divergence is used as the minimization function in the optimization method.
370 After preliminary experiments, we found out that 5 generations in the genetic algorithm were
371 enough to give a well suited initial guess for the newUOA algorithm (i.e. the changes in the
372 parameters between generations were smaller than 4%).

373 The third set of experiments explores the Jensen-Shannon divergence for imperfect models. In
374 this case the observed time series is obtained from a 'nature' integration of the two-scale Lorenz
375 '96 system, and we seek to reproduce the dynamics of the system with integrations of imperfect
376 models generated from one-scale Lorenz '96 systems with deterministic and stochastic parame-
377 terizations. From these experiments we determine a set of optimal values using the mentioned
378 optimization method for a deterministic and stochastic parameterization that seek to represent the
379 small-scale dynamical effects of the two-scale Lorenz '96 system. These optimal parameter values
380 are used in long-term climate prediction experiments to examine whether the optimal parameters
381 have a positive impact on climate measures.

382 **4. Results and discussion**

383 *a. Experiments with the two-scale Lorenz '96 system*

384 First, the ordinal symbolic analysis is applied to the integration of what we consider as the nat-
385 ural system evolution, the two-scale Lorenz '96 system. Integrations varying the forcing F were

386 conducted with a resolution of $\delta F = 0.01$, and the ordinal symbolic analysis is applied to each
 387 integration (i.e. time series of the Lorenz '96 variable X_1). Figure 1 shows the information quan-
 388 tifiers: permutation entropy (\mathcal{H} , Fig. 1a), permutation statistical complexity (\mathcal{C} , Fig. 1b). From
 389 Figs. 1a and 1b, four regions with different dynamical regimes are found (which are delimited by
 390 vertical dotted lines): (i) For small external forcing, $0 \leq F \leq 3.75$, the system is dissipative and so
 391 after the spin-up time the entropy goes to zero. (ii) A narrow region, between $3.75 < F < 4.5$, with
 392 high permutation entropy and high permutation statistical complexity. (iii) An intermediate region,
 393 between $5 < F < 12$, with small entropy $\mathcal{H} \approx 0.2 - 0.23$ and similar complexity. (iv) Finally a
 394 region for larger F , $F > 13$, which has large entropy $\mathcal{H} > 0.4$ but relatively small complexity
 395 ($\mathcal{C} < 0.4$).

396 Figure 1c shows the causal entropy-complexity plane ($\mathcal{H} \times \mathcal{C}$) which combines the entropy and
 397 statistical complexity measures. In this plane, the statistical complexity has a minimum and max-
 398 imum value as a function of entropy (\mathcal{C}_{min} and \mathcal{C}_{max} respectively), which are the upper and lower
 399 continuous curves in Fig. 1c, so that all the possible dynamical regimes are limited to the area
 400 between these curves. The four dynamical regimes can be clearly distinguished in the entropy-
 401 complexity plane. The dissipative regime is located at the extreme of null entropy and complexity.
 402 The regime (ii) is represented with gray triangles (with black contours), which corresponds to
 403 the narrow region between $3.75 < F < 4.5$ with large entropy and maximal complexity (at the
 404 \mathcal{C}_{max} curve). The quasi-periodic dynamical regime (iii) with low entropy and maximal statistical
 405 complexity is denoted by the black triangles that are close to the upper curve which represents
 406 the maximal statistical complexity. The large F chaotic regime (iv) which has large entropy and
 407 relatively small complexity is represented with gray circles. Since the system is purely determin-
 408 istic, there are no dynamical regimes in the large entropy region, close to $\mathcal{H} = 1$, which would
 409 represent a purely stochastic system (Rosso et al. 2007).

410

411

412 Figure 2 shows the time series, resulting from the dynamical regimes obtained from the two-
413 scale Lorenz '96 dynamical system (except the dissipative regime) identified using the information
414 quantifiers, for $F = 4$ (Figure 2a), $F = 7$ (Figure 2b) and $F = 18$ (Figure 2c). These represent quasi-
415 periodic motion with high entropy, quasi-periodic motion with low entropy and chaotic motion,
416 respectively.

417 Figure 3 shows the information quantifiers from integrations of the two-scale Lorenz '96 system
418 varying the coupling constant h . The external forcing is fixed to $F = 4, 6, 18$. For $h \rightarrow 0$ we recover
419 the measures for the one-scale Lorenz '96 system since the two sets of equations, (11) and (12), are
420 uncoupled. In that case, the permutation entropy and the permutation statistical complexity scales
421 with the forcing. For $F = 4$, there is a peak of entropy and complexity when the coupling constant
422 h is close to 1, which was the regime already found in Fig. 1 with complexity close to \mathcal{C}_{max} (note
423 that in those integrations $h = 1$). For coupling constants larger than $h > 1.2$, the large-scale and
424 small-scale states are constants (note that the amplitude of oscillations for $F = 4$ and $h = 1$ in Fig.
425 2a is very small). As we increase F to 6, the large complexity regime is found for larger coupling
426 between the two scales, for h between 1.4 and 2. On the other hand, small entropy and complexity
427 is found for the $F = 18$ for coupling constants between 1 and 2. For larger coupling constants, a
428 regime with high disordered patterns is found (small complexity and large entropy). For coupling
429 constants close to 5, a regime with high statistical complexity appears to emerge for the $F = 18$ but
430 we did not explore integrations for larger coupling constants. Some of the dynamical regimes that
431 appear to emerge from the Lorenz '96 system varying the coupling constant and varying stochastic
432 noise will be investigated further in a follow-up work.

433

434 *b. Perfect-model experiments*

435 To evaluate the potential of information quantifiers to distinguish between time series generated
436 with different parameterizations, we conducted a so-called twin experiment. We consider the one-
437 scale Lorenz '96 system, (13), with a known parameterization as the natural system evolution to
438 generate the observed time series and then we evaluate the information measures for integrations
439 of the one-scale Lorenz '96 system with varying parameters using the hybrid optimization algo-
440 rithm, with genetic algorithm and newUOA methods. This is an experiment where the model is
441 assumed perfect, and a set of prescribed parameters are used to generate the observations. Then,
442 the optimization method is used to estimate the parameters through the differences in the observed
443 and modeled time series. In this way, we can evaluate whether the Jensen-Shannon divergence
444 measure determined with the ordinal symbolic analysis is able to estimate the “true” parameters.

445 The first perfect model experiment uses a deterministic quadratic parameterization, (14) in the
446 system (13). The true parameter values are set to $a_0^t = 17.0$, $a_1^t = -1.20$, $a_2^t = 0.035$ (t superscript
447 denotes true values). These values are expected to be a representative deterministic parameter-
448 ization of the two-scale model (Pulido et al. 2016). In this perfect-model experiment with the
449 system (13), there is no constant forcing but a quadratic forcing. The resulting dynamical regime
450 from (13) with quadratic forcing ($a_0^t = 17.0, a_1^t = -1.20, a_2^t = 0.035$) is expected to be like an
451 $F = 17 - 18$ constant forcing. The integration with the true parameters is considered as the ob-
452 servational time series. The Jensen-Shannon divergence, (10) is minimized through the hybrid
453 optimization algorithm which seek for the optimal model parameter values. The symbolic ordinal
454 analysis is applied to each model and observational time series to evaluate the Jensen-Shannon
455 divergence, (10). The optimal parameter values obtained with the hybrid optimization algorithm
456 were $a_0 = 17.1$, $a_1 = -1.18$ and $a_2 = 0.032$. This twin experiment shows that the information

457 measures can be used to determine optimal parameters, the estimated optimal values are very
458 close to the true parameter values. In preliminary experiments, we also evaluated the Hellinger
459 divergence (e.g. Arnold et al. 2013) as an alternative to Jensen-Shannon divergence. Both distance
460 measures performed similarly well, so that we only show the experiments with Jensen-Shannon
461 divergence.

462 The sensitivity in the Jensen-Shannon divergence to the parameters is shown in Fig. 4 varying
463 each of the parameters and the other two parameters are fixed to the optimal values (which were
464 obtained with the hybrid optimization method using Jensen-Shannon divergence). The optimal
465 parameter is very well defined in the three parameters. The minimum of the Jensen-Shannon di-
466 vergence is clearly located at the true parameters. One weak point of the measure is that it presents
467 noise, including several local extremes. This affects the convergence speed of optimization meth-
468 ods.

469 A second perfect-model experiment takes a stochastic parameterization, (15), for the polyno-
470 mial coefficients we use the same true values as in the previous experiment, $a_0^t = 17$, $a_1^t = -1.2$,
471 $a_2^t = 0.035$ but we now include a noise forcing term with standard deviation $\sigma^t = 1$. Two op-
472 timization experiments with autoregressive parameters $\phi^t = 0$ and $\phi^t = 0.984$ were conducted.
473 These two extreme values were taken by Wilks (2005) to represent serially independent and se-
474 rially persistent stochastic forcing, respectively. The resulting optimal parameter values of the
475 hybrid optimization algorithm are shown in Table 1. The combined estimation of deterministic
476 parameters and the stochastic parameter σ gives rather good estimates. The stochastic parameter
477 is slightly underestimated by 10-20% in the two optimization experiments.

478 Once the optimal parameters for the stochastic parameterization are estimated, we then evaluate
479 the sensitivity of Jensen-Shannon divergence measure with respect to this observational time se-
480 ries varying σ values in the model integrations. Figure 5 depicts the Jensen-Shannon divergence

481 as a function of σ parameter for autoregressive parameters of $\phi^t = 0$ and $\phi^t = 0.984$ (the other
482 parameters are fixed to the optimal values that were estimated with the hybrid optimization algo-
483 rithm). A rather narrow negative peak is found in Fig. 5 close to the true parameter values. The
484 $\phi^t = 0.984$ case (Fig. 5b) appears to be better conditioned.

485

486 *c. Imperfect-model experiments*

487 The usual procedure to infer unknown parameters of a parameterization scheme in an imper-
488 fect, coarse-grained, model is to tune the unknown parameters and to evaluate the response of
489 the changes in the parameters on the root-mean-square error, which measures the differences be-
490 tween the evolution of some representative variables and the corresponding observed variables (or
491 reanalysis data). The optimal parameters are the ones that minimize the root-mean-square error.
492 We conducted a similar experiment with synthetic observations but using information measures,
493 i.e. Jensen-Shannon divergence, instead of root-mean-square error measures. The advantage of
494 the ordinal symbolic analysis is that as it does not depend on the amplitude but on the “shape” of
495 the patterns, it is not sensitive to possible systematic model errors. The analysis is performed in a
496 sufficiently long trajectory (10^5 observational times). The probability of all the possible patterns
497 is composed by a large number of cases and it is expected to be independent of the initial con-
498 dition (the spin-up time is not considered in the statistics). The observed time series corresponds
499 to a single variable taken from a model integration of the two-scale Lorenz '96 system which is
500 started from random initial conditions and the spin-up period is removed. The model time series
501 is also generated from random initial conditions and integrating the one-scale Lorenz '96 sys-
502 tem. Therefore, the two time series are completely independent—they do not have a common

503 initial condition. In this sense, the Jensen-Shannon divergence is a global measure of the system
504 dynamics.

505 Since we deal with an imperfect model, which does not represent explicitly the small-scale
506 dynamics, the parameter estimation is not a twin experiment in which we know the “true” optimal
507 parameters, so that the existence of a single set of optimal parameters is not a priori ensured.

508 We conducted two extreme experiments, one with the natural system evolution set for an external
509 forcing of $F = 7$, which results in quasi-periodic motion, and the other for a forcing of $F = 18$,
510 which results in chaotic dynamical behavior. As mentioned, the ordinal symbolic analysis may
511 be applied to chaotic and quasi-periodic time series as long as the weak stationary assumption is
512 satisfied.

513 The hybrid optimization algorithm was applied to the two observed time series. The genetic
514 algorithm restricts the search for optimal values to the region delimited by the maximum and
515 minimum values stated in Table 2. The parameter limits (maximum and minimum values) of the
516 search region were taken according to the values obtained by Pulido et al. (2016). In the case that
517 the resulting optimal value of the genetic algorithm is at a boundary of the region, it is an indicative
518 that the region is too narrow in that parameter and that the limit value should be changed. The
519 estimated optimal values with the hybrid optimization algorithm for $F = 7$ and $F = 18$ are also
520 shown in Table 2.

521 The Jensen-Shannon divergence sensitivity to each of the parameter values for the case $F = 7$,
522 varying one parameter value and fixing the other two to the optimal values which resulted from
523 the hybrid optimization algorithm, is shown in Fig. 6. Parameters exhibit strong sensitivity in
524 a small region close to the optimal values. These sensitivity experiments are produced after the
525 optimization, with independent integrations that are not related to the optimization method. For
526 some parameter values, the Lorenz '96 model presents numerical instabilities. A uniform time

527 series is assigned for these cases and so a delta PDF results, which in turn gives a large Jensen-
528 Shannon divergence.

529 The sensitivity of the Jensen-Shannon divergence to each of the parameters for the case of
530 $F = 18$ is shown in Fig. 7, while the other two parameters are fixed at the optimal values. The
531 parameter a_0 exhibits a reasonable sensitivity around the optimal value. On the other hand, a_1
532 and a_2 show several peaks so that they are more difficult to be precisely estimated, however, the
533 genetic algorithm is clearly able to find the global minimum even in the presence of these local
534 minima (Fig. 7c).

535

536

537 As the information quantifiers give useful information on the optimal parameter values of the
538 deterministic parameterization, we now turn our attention to stochastic parameterizations for the
539 imperfect case. We include the first-order autoregressive process (16) in the parameterization (15),
540 and search with the hybrid optimization algorithm for the optimal parameter values including the
541 optimal standard deviation σ , (a_0, a_1, a_2, σ) , and again we only explore for two fixed autore-
542 gressive parameters $\phi = 0$ and $\phi = 0.984$. The resulting optimal parameter values of the hybrid
543 optimization algorithm are shown in Table 2.

544 The Jensen-Shannon divergence as a function of the standard deviation is depicted in Fig. 8 for
545 the optimal deterministic parameter values (shown in Table 2). For an external forcing of $F = 7$ a
546 smooth function is found with a clear minimum (see Fig. 8a). The minimum is found at $\sigma = 0.32$
547 for $\phi = 0$. Similar values of the Jensen-Shannon divergence are found at $\sigma = 0.15$ for $\phi = 0.984$.
548 Both sets of values are suitable for representing the stochastic process that mimics the effects
549 of Lorenz'96 small-scale variables. Note that the Jensen-Shannon divergence for the optimal
550 σ value is smaller than the one for $\sigma = 0$ so that the stochastic parameterization improves the

551 representation of small-scale variables. This is also valid when both deterministic and stochastic
552 parameterizations have their own optimal parameters.

553 For $F = 18$ Jensen-Shannon divergence has smaller values than $F = 7$. This means that the
554 parameterization is able to represent better the effects of the small-scale variables for this case due
555 to the chaotic dynamics. The divergence depicts a noisy dependence, but a constrained optimal
556 range of the standard deviation is still clearly identified from Fig. 8b. There is an optimal range for
557 $4 < \sigma < 6$ with similar D_{JS} values in which the parameterization is practically indistinguishable.
558 Similar Jensen-Shannon divergence values are also found for the $\phi = 0.984$ experiment with with
559 a more constrained minimum (better conditioned Jensen-Shannon divergence) at about $\sigma = 2.1$.

560 To evaluate the information quantifiers as a method for model selection. We conducted an ex-
561 periment in which we assume that the model has different parameterizations, changing the order
562 of the polynomial function in the deterministic parameterization and for some experiments adding
563 the stochastic process (16). A total of eight optimization experiments with different parameteri-
564 zations were conducted for an observed time series taken from the two-scale Lorenz '96 system
565 with $F = 18$. For each parameterization, the set of optimal parameters estimated by the hybrid
566 optimization algorithm are stated in Table 3. The square root of Jensen-Shannon divergence for
567 the optimal parameters is also shown in the Table. The best parameterization is the one that gives
568 the minimal Jensen-Shannon divergence from the observed PDF. The quadratic polynomial pa-
569 rameterization is the best deterministic one. Interestingly, the stochastic parameterizations present
570 a significantly better performance with this information measure. The higher-order polynomial
571 terms are very sensitive to small changes in the variables and parameters and for some parameter
572 values they produce numerical instabilities in the Lorenz '96 model (Pulido et al. 2016). Indeed,
573 the optimization experiment with the fourth-order polynomial stochastic parameterization did not

574 converge towards optimal parameter values because of these ubiquitous numerical instabilities (to
575 overcome this, careful manual changes in the parameter limit values would be required).

576 The forcing given by the parameterizations with optimal parameters for the $F = 18$ experiments,
577 including the quadratic deterministic, and the quadratic stochastic parameterizations with $\phi = 0$
578 and with $\phi = 0.984$ are shown in Fig. 9 (Panels (a), (b) and (c) respectively). The forcing given
579 by the small-scale variables in the two-scale Lorenz '96 is also shown in the Figure (gray dots).
580 We emphasize, this “true” forcing is only shown as the purpose of evaluation of the optimization
581 experiments, but the time series of a single large-scale state variable is the only source of infor-
582 mation used in the optimization experiments. The simple polynomial parameterizations with fixed
583 standard deviation represent rather well the complex forcing dependencies given by the small-
584 scale variable. However, they are obviously unable to represent the dependence of the standard
585 deviation with the value of the state variable particularly at the tail (large X values) and with the
586 $dX/dt > 0$ and $dX/dt < 0$ branches of the forcing, see Crommelin and Vanden-Eijnden (2008);
587 Pulido et al. (2016).

588 As an independent measure of the climatology of the model with optimal parameters, we use
589 the classical histogram PDF. They were computed from the whole integration with the different
590 optimal parameter values. Figure 10 shows the histogram PDF for the nature integration for $F = 18$
591 and the ones with the optimal parameters for the quadratic deterministic parameterization (dashed
592 line) and for the stochastic parameterizations using $\phi = 0$ (dotted line) and $\phi = 0.984$ (gray line).
593 A very good agreement between the true histogram PDF and the model PDF is achieved. The
594 stochastic parameterizations give a slightly better agreement to the true histogram PDF.

595 **5. Conclusions**

596 Ordinal symbolic analysis only depends on the repetition of patterns within a time series. If it
597 is combined with information measures, they represent a useful framework to evaluate models, in
598 particular unresolved processes of multi-scale models. Since ordinal symbolic analysis does not
599 depend directly on the state, the quantities can be used for long time intervals (time series) even
600 in the presence of model error. The ordinal symbolic analysis is used in this work for long time
601 series and it accounts for the model fidelity with strong sensitivity to the parameters of the subgrid
602 parameterization which represents the small-scale processes.

603 Although stochastic parameterizations appear to give improvements in the atmospheric numeri-
604 cal models, the tuning of stochastic parameters represents a challenge. On-line parameter estima-
605 tion techniques as Kalman filtering present difficulties estimating these stochastic parameters even
606 for small and intermediate systems. DelSole and Yang (2010) show that it is not possible to con-
607 strain stochastic parameters with ensemble-based Kalman filters augmenting the model state with
608 the stochastic parameters. Ruiz et al. (2013b) show that a separate adaptive inflation treatment
609 is required for the parameter covariance to avoid its collapse. Pulido et al. (2016) show that the
610 time variability given by Kalman filtering parameter estimates is not useful to constrain stochastic
611 parameters in a subgrid parameterization. In this work, we show that information measures from
612 ordinal symbolic analysis are useful for tuning stochastic parameters with promising results.

613 This work evaluates the sensitivity of the parameters to the information measures, which is use-
614 ful for model selection. Furthermore, for parameter optimization a hybrid optimization technique
615 using a genetic and newUOA algorithms was implemented in this work for low dimensional mod-
616 els. For some cases, the information measures based on the ordinal symbolic analysis do not give
617 smooth dependencies with the parameters. This may be a problem for traditional gradient descent

618 optimization methods. For parameter estimation in high-dimensional models more sophisticated
619 optimization techniques suitable for noisy cost functions, like simulated annealing, or stochastic
620 gradient descent, are required to minimize the Jensen-Shannon divergence for the probability dis-
621 tributions of observations and an imperfect model. The evaluation of optimization techniques in
622 high-dimensional models with information measures will be examined in a follow-up work.

623 The proposed parameter estimation method offers an alternative framework to methods that
624 couple model state to observations like for instance data assimilation. On the other hand, in the
625 proposed method the model time series is generated independently of the observed state of the
626 system. The model state is assumed to be in its own model attractor (which is not necessarily
627 the one from nature). Only partial observation of the system is needed, indeed the observed time
628 series may be a single relevant variable or a small set of variables. The information measures could
629 be applied to a set of *free* integrations from different climate models or a set of *free* integrations
630 from a single climate model with different parameterizations or parameters, to evaluate from an
631 observed time series, which climate model or parameterization give the most accurate results—the
632 closest PDF to the observed PDF.

633 This work evaluates the information measures with the Lorenz'96 system, which is a small
634 model with 8 – 256 variables. Two major points need to be evaluated with more realistic models,
635 the impact of a higher-dimensional state space on the information measures, and the length of the
636 time series needed to compute the probability distributions. The length of the time series used in
637 this work would represent about 70 years in the atmospheric time scale. It depends on two factors,
638 the required time resolution and the length of the pattern used for the ordinal symbolic analysis.
639 The time resolution used in this work is related to the time-scale of the resolved large-scale pro-
640 cesses, and indeed the used time series corresponds to a large-scale variable. The length of the
641 sequence is taken to be six in this work, as used in other applications Sippel et al. (2016); Seri-

642 naldi et al. (2014). However, Tirabassi and Massoller (2016) used three for monthly climate time
643 series (which are of limited length) with meaningful results. The way to combine the information
644 measures of different variables for high-dimensional problems needs to be explored.

645 The information measures can deal with weak observational noise (Rosso et al. 2007), how-
646 ever as expected Shannon entropy gives a maximum if the time series is stochastic without
647 correlations— completely dominated by white noise. For the cases with strong observational
648 noise, the signal may not be useful for analyzing fast processes, but averaging the time series and
649 applying ordinal symbolic analysis in longer time steps may give useful information for slower
650 physical processes.

651 *Acknowledgments.* We are grateful to three anonymous reviewers for their valuable comments.
652 We acknowledge CONICET Grant PIP 112-20120100414CO which funded a two-week visit of
653 one of us (MP) to the Universidade Federal de Alagoas.

654 **References**

655 Abarbanel H. D. I., 1996: *Analysis of observed chaotic data*. Springer-verlag, New York.

656 Aksoy, A., 2015: Parameter Estimation. In: G. R. North (editor-in-chief), J. Pyle and F. Zhang
657 (editors). *Encyclopedia of Atmospheric Sciences*, 2nd edition, **4**, 181–186.

658 Arnold H.M., Moroz I.M., Palmer T.N., 2013: Stochastic parametrizations and
659 model uncertainty in the Lorenz 96 system. *Phil Trans R Soc A*, **371**, 20110479.
660 <http://dx.doi.org/10.1098/rsta.2011.0479>

661 Bandt, C. and Pompe, B., 2002: Permutation entropy: a natural complexity measure for time
662 series. *Phys. Rev. Lett.*, **88**, 174102.

- 663 Bollt E., T. Stanford, Y.-C. Lai, and K. Zyczkowski, 2000: Validity of threshold-crossing analysis
664 of symbolic dynamics from chaotic time series, *Phys. Rev. Lett.* **85**, 3524.
- 665 Brissaud J. B., 2005: The meanings of entropy. *Entropy*, **7**, 68-96.
- 666 Charbonneau P. 2002. An introduction to genetic algorithms for numerical optimization. Technical
667 Note TN-450+IA. NCAR: Boulder, MA.
- 668 Christensen, H.M., I. M. Moroz and T. N. Palmer, 2015: Stochastic and perturbed parameter
669 representations of model uncertainty in convection parameterization. *J. Atmos. Sci.*, **72**, 2525–
670 2544.
- 671 Crommelin, D. and Vanden-Eijnden, E., 2008. Subgrid-scale parameterization with conditional
672 Markov chains. *J. Atmos. Sci.*, **65**, 2661-2675.
- 673 DelSole, T., and X. Yang., 2010: State and parameter estimation in stochastic dynamical models.
674 *Physica D*, **239**, 1781–1788.
- 675 Eckmann J. -P., Ruelle D., 1985: Ergodic theory of chaos and strange attractors. *Rev. Mod. Phys.*,
676 **57**, 617–656.
- 677 Gray, R.M., 1990: *Entropy and Information Theory*. Springer, Berlin-Heidelberg, Germany.
- 678 Grosse I., Bernaola-Galván P., Carpena P., Román-Roldán R., Oliver J. and Stanley H.E., 2002:
679 Analysis of symbolic sequences using the Jensen-Shannon divergence. *Phys. Rev. E*, **65** 041905.
- 680 Kantz H., Kurths J., Meyer-Kress G., 1998: *Nonlinear Analysis of Physiological Data*, Springer,
681 Berlin
- 682 Khinchin I., 1957: *Mathematical foundations of the information theory*. Dover Publ. New York.

- 683 Klinker, E. and P. Sardeshmukh, 1992: The diagnosis of mechanical dissipation in the atmosphere
684 from large-scale balance requirements. *J. Atmos. Sci.*, **49**, 608-627.
- 685 Lang M., P. J. Van Leeuwen, and P. Browne, 2016: A systematic method of parameterisation
686 estimation using data assimilation. *Tellus*, **68**, 29012.
- 687 Lamberti, P. W., Martín, M. T., Plastino, A., and O. A. Rosso, 2004: Intensive entropic non-
688 triviality measure. *Physica A*, **334**, 119–131.
- 689 Leung, L.-Y., and G. R. North, 1990: Information theory and climate prediction. *J. Climate*, **3**,
690 5–14.
- 691 Lin J 1991: Divergence measures based on the Shannon Entropy *IEEE Transactions on Informa-*
692 *tion Theory*, **37**, 145-151.
- 693 López-Ruiz R., Mancini H.L., Calbet X., 1995: A statistical measure of complexity. *Phys. Lett. A*,
694 **209**, 321–326.
- 695 Lorenz, E. N., 1996: Predictability— A problem partly solved. In *Proc. Seminar on Predictabil-*
696 *ity*, Shinfield Park, Reading, United Kingdom, European Centre for Medium-Range Weather
697 Forecasting, 1-18.
- 698 Lott, F., L. Guez, and P. Maury, 2012: A stochastic parameterization of non-orographic gravity
699 waves: Formalism and impact on the equatorial stratosphere. *Geophys. Res. Lett.* **39**, L06807,
700 doi:10.1029/2012GL051001.
- 701 Majda, A.J. and Gershgorin, B., 2011: Improving model fidelity and sensitivity for complex sys-
702 tems through empirical information theory. *Proceedings of the National Academy of Sciences*,
703 **108**, 10044–10049.

- 704 Martín M.T., Plastino A., Rosso O.A., 2006: Generalized statistical complexity measures: Geo-
705 metrical and analytical properties. *Physica A*, **369**, 439–462.
- 706 Palmer, T. N., 2001: A nonlinear dynamical perspective on model error: A proposal for non-
707 local stochastic-dynamic parameterization in weather and climate prediction models. *Q. J. Roy.*
708 *Meteor. Soc.*, **127**, 279–304.
- 709 Pesin Ya. B., 1977: Lyapunov characteristic exponents and smooth ergodic theory. *Usp. Mat.*
710 *Nauk.*, **32**, 55.
- 711 Piani, C., W. A. Norton, and D. A. Stainforth, 2004: Equatorial stratospheric response to variations
712 in deterministic and stochastic gravity wave parameterizations. *J. Geophys. Res.*, **109**, 1984–
713 2012.
- 714 Powell, M.J., 2006. The NEWUOA software for unconstrained optimization without derivatives.
715 In *Large-scale nonlinear optimization*. 255-297. Springer.
- 716 Pulido M, Polavarapu S, Shepherd TG, Thuburn J. 2012. Estimation of optimal gravity wave pa-
717 rameters for climate models using data assimilation. *Quart. J. R. Meteorol. Soc.*, **138**, 298-309.
- 718 Pulido, M, 2014: A simple technique to infer the missing gravity wave drag in the middle atmo-
719 sphere using a general circulation model: Potential vorticity budget. *J. Atmos. Sci.*, **71**, 683-696.
- 720 Pulido M., G. Scheffler, J. Ruiz, M. Lucini and P. Tandeo, 2016: Estimation of the functional form
721 of subgrid-scale schemes using ensemble-based data assimilation: a simple model experiment.
722 In press *Q. J. Roy. Meteorol. Soc.* DOI: 10.1002/qj.2879.
- 723 Rodwell, M.J., and T. N. Palmer, 2007: Using numerical weather prediction to assess climate
724 models. *Q. J. Roy. Meteor. Soc.*, **33**, 129-146.

- 725 Rosso, O. A., Larrondo, H. A., Martín, M. T., Plastino, A., and M. A. Fuentes, 2007: Distinguish-
726 ing noise from chaos. *Phys. Rev. Lett.*, **99**, 154102.
- 727 Rosso O. A. and Masoller C., 2009: Detecting and quantifying stochastic and coherence reso-
728 nances via information-theory complexity measurements. *Phys. Rev. E*, **79**, 040106(R).
- 729 Rosso O. A. and Masoller C., 2009: Detecting and quantifying temporal correlations in stochastic
730 resonance via information theory measures. *Eur. Phys. J. B*, **69**, 37–43.
- 731 Rosso O.A., Carpi L.C., Saco P.M., Gómez Ravetti M., Plastino A., Larrondo H., 2012: Causality
732 and the Entropy-Complexity Plane: Robustness and Missing Ordinal Patterns. *Physica A*, **391**,
733 42–55.
- 734 Rosso O.A., Carpi L.C., Saco P.M., Gómez Ravetti M., Larrondo H., Plastino A., 2012: The
735 Amigó paradigm of forbidden/missing patterns: a detailed analysis *Eur. Phys. J. B* **85**, 419–430.
- 736 Ruiz J., M. Pulido and T. Miyoshi, 2013: Estimating parameters with ensemble-based data assim-
737 ilation. A review. *J. Meteorol. Soc. Japan*. **91**, 79–99.
- 738 Ruiz J., M. Pulido and T. Miyoshi, 2013: Estimating parameters with ensemble-based data assim-
739 ilation. Parameter covariance treatment. *J. Meteorol. Soc. Japan*. **91**, 453-469.
- 740 Ruiz J. and M. Pulido, 2015: Parameter estimation using ensemble based data assimilation in the
741 presence of model error. *Mon. Wea. Rev.*, **143**, 1568–1582.
- 742 Serinaldi F., L. Zunino, O. A. Rosso, 2014: Complexity-entropy analysis of daily stream flow time
743 series in the continental United States. *Stoch. Environ. Res. Risk Assess.*, **28**, 16851708
- 744 Shannon C.E., 1948: A mathematical theory of communication. *Bell Syst. Technol. J.*, **27**, 379–
745 423, 623–656.

- 746 Shannon C.E. and Weaver W., 1949: The Mathematical Theory of Communication, University of
747 Illinois Press, Champaign, IL, USA.
- 748 Schuster, H.G. and Just, W., 2006. *Deterministic chaos: an introduction*. John Wiley and Sons.
- 749 Shutts, G., 2005: A kinetic energy backscatter algorithm for use in ensemble prediction systems.
750 *Q. J. R. Meteorol. Soc.* **131**, 3079–3102.
- 751 Sippel S., Lange H., Mahecha M.D., Hauhs M., Bodesheim P., Kaminski T., Gans F. and Rosso
752 O. A., 2016: Diagnosing the Dynamics of Observed and Simulated Ecosystem Gross Primary
753 Productivity with Time Causal Information Theory Quantifiers. *PLoS ONE*, **11**, e0164960.
754 doi:10.1371/journal.pone.0164960
- 755 Stainforth D.A., T. Aina, C. Christensen, M. Collins, N. Faull, D. J. Frame, J. A. Kettleborough,
756 S. Knight, A. Martin, J. M. Murphy, C. Piani, D. Sexton, L. A. Smith, R. A. Spicer, A. J. Thorpe
757 and M. R. Allen, 2005: Uncertainty in predictions of the climate response to rising levels of
758 greenhouse gases, *Nature*, **433**, 403–406. doi:10.1038/nature03301
- 759 Tirabassi and Massoller C. 2016: Unravelling the community structure of the climate system by us-
760 ing lags and symbolic time-series analysis. *Scientific Reports* , **6** 29804. doi:10.1038/srep29804
- 761 Wilks D. S., 2005: Effects of stochastic parameterizations in the Lorenz 96 system. *Q. J. R. Mete-*
762 *orol. Soc.*, **131**, 389–407. doi: 10.1256/qj.04.03
- 763 Zanin M., Zunino L., Rosso O. A. and Papo D., 2012: Permutation entropy and its main biomedical
764 and econophysics applications: A review. *Entropy*, **14**, 1553–1577.

765 **LIST OF TABLES**

766 **Table 1.** Values of the parameters (a_i , i degree of the polynomial term and standard de-
767 viation, σ) for the quadratic stochastic parameterization in the perfect-model
768 experiment. The true values correspond to the values used to generate the ob-
769 servations. The optimal values obtained with the hybrid optimization algorithm
770 for $\phi^t = 0$ and $\phi^t = 0.984$ experiments. 37

771 **Table 2.** Values of the parameters (a_i , i degree of the polynomial term and σ). The max-
772 imum and minimum values used to constrain the optimization and the optimal
773 values obtained with the hybrid optimization algorithm corresponding to the
774 deterministic (Det), $\phi = 0$ and $\phi = 0.984$ experiments. 38

775 **Table 3.** Estimated values of the parameters (a_i , i degree of the polynomial term, and
776 stochastic parameter σ) for the deterministic and stochastic parameterizations
777 with $\phi = 0$ in the imperfect-model experiment. 39

	a_0	a_1	a_2	σ
True Values	17.0	-1.20	0.035	1.0
$\phi_T = 0$	17.0	-1.17	0.031	0.82
$\phi_T = 0.984$	17.0	-1.19	0.034	0.88

778 TABLE 1. Values of the parameters (a_i , i degree of the polynomial term and standard deviation, σ) for the
779 quadratic stochastic parameterization in the perfect-model experiment. The true values correspond to the values
780 used to generate the observations. The optimal values obtained with the hybrid optimization algorithm for $\phi^f = 0$
781 and $\phi^f = 0.984$ experiments.

Coef	$F = 7$					$F = 18$				
	Min	Max	Det	$\phi = 0$	$\phi = 0.984$	Min	Max	Det	$\phi = 0$	$\phi = 0.984$
a_0	2.0	8.0	5.79	5.78	6.97	14.0	19.0	17.7	18.5	17.1
a_1	-3.5	0.0	-2.79	-1.76	-2.18	-3.0	0.0	-1.19	-1.28	-1.26
a_2	0.0	0.8	0.50	0.22	0.25	0.0	0.5	0.038	0.039	0.049
σ	0.0	2.0		0.32	0.15	0.0	5.0		4.67	2.13

782 TABLE 2. Values of the parameters (a_i , i degree of the polynomial term and σ). The maximum and minimum
783 values used to constrain the optimization and the optimal values obtained with the hybrid optimization algorithm
784 corresponding to the deterministic (Det), $\phi = 0$ and $\phi = 0.984$ experiments.

	a_0	a_1	a_2	a_3	a_4	σ	$\sqrt{D_{JS}}$
Linear	18.36	-0.981					0.3950E-01
Quadratic	17.7	-1.19	0.038				0.3224E-01
Cubic	18.6	-1.50	0.062	0.0002			0.3434E-01
Quartic	18.2	-1.35	0.094	-0.0046	0.00007		0.3309E-01
Linear	19.1	-1.00				3.83	0.3120E-01
Quadratic	18.5	-1.28	0.039			4.67	0.2910E-01
Cubic	17.1	-1.15	0.073	-0.0033		1.49	0.3050E-01

785 TABLE 3. Estimated values of the parameters (a_i , i degree of the polynomial term, and stochastic parameter
786 σ) for the deterministic and stochastic parameterizations with $\phi = 0$ in the imperfect-model experiment.

787 **LIST OF FIGURES**

788 **Fig. 1.** (a) Permutation entropy (\mathcal{H}), (b) permutation statistical complexity (\mathcal{C}), and (c) the causal
789 entropy-complexity plane ($\mathcal{H} \times \mathcal{C}$) for two-scale Lorenz '96 integrations as a function of
790 the forcing F with a resolution of $\delta F = 0.01$. Vertical dotted lines in (a) and (b) divide
791 the four dynamical regimes found. The minimal and maximal complexity values, \mathcal{C}_{min} and
792 \mathcal{C}_{max} as a function of permutation entropy are shown with black solid curves in panel (c).
793 Regime (i) represents a dissipative system, (ii) quasi-periodic regime with high entropy, (iii)
794 quasi-periodic with low entropy and (iv) chaotic regime. The transition points between the
795 regions are not represented in panel (c) to improve visibility of the different regimes. The
796 coupling factor in these experiments is $h = 1$ 41

797 **Fig. 2.** Time series of a two-scale Lorenz '96 variable for (a) $F = 4$, (b) $F = 7$, and (c) $F = 18$ 42

798 **Fig. 3.** (a) Permutation entropy (\mathcal{H}), (b) permutation statistical complexity (\mathcal{C}), and (c) the causal
799 entropy-complexity plane ($\mathcal{H} \times \mathcal{C}$) for two-scale Lorenz '96 integrations with varying cou-
800 pling constant h in steps of $\delta h = 0.1$ for $F = 4$ (continuous line, circle points), $F = 6$ (dotted
801 curves, square points) and $F = 18$ (dashed curves, triangle points). 43

802 **Fig. 4.** Jensen-Shannon divergence as a function of a_0 , a_1 and a_2 under the perfect model assump-
803 tion. The true parameter values are shown with vertical dotted lines. The square root of
804 Jensen-Shannon divergence is used to make visible small values close to the minimum. 44

805 **Fig. 5.** Jensen-Shannon divergence as a function of the standard deviation, σ , and autoregressive
806 parameter values (a) $\phi^t = 0$, and (b) $\phi^t = 0.984$ for the perfect model experiments. The
807 other parameters are kept fixed at the optimal values. 45

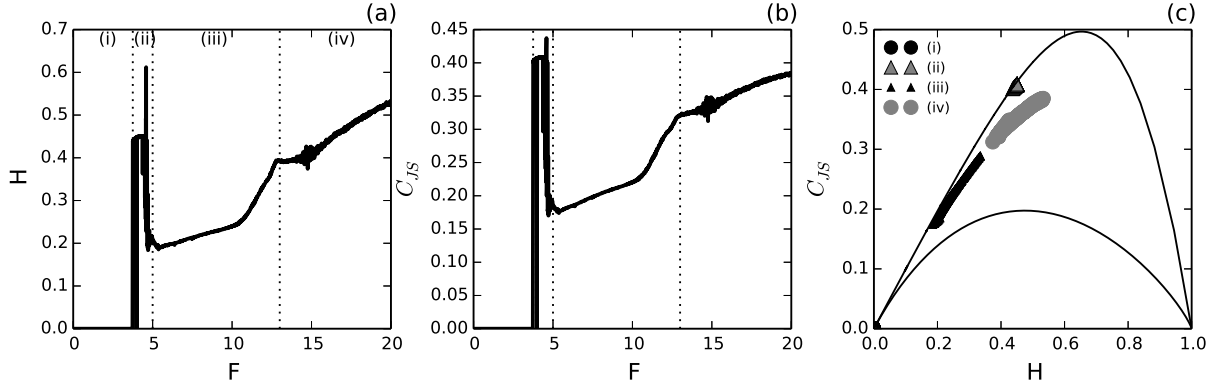
808 **Fig. 6.** Jensen-Shannon divergence between the probability distribution from the model integration
809 with a given set of parameters, and the one from the natural two-scale Lorenz '96 system
810 evolution for an external forcing of $F = 7$. Two parameters are kept fixed at the estimated
811 values (Table 2) and the third one is varied: a) a_0 , b) a_1 , and c) a_2 dependencies. Vertical
812 dotted lines show the optimal parameter values. 46

813 **Fig. 7.** Jensen-Shannon divergence between the probability distribution from the model integration
814 with a given set of parameters, and the one from the natural two-scale Lorenz '96 system
815 evolution for an external forcing of $F = 18$. One parameter value is varied and the other two
816 are kept fixed at the optimal values (Table 2), (a) a_0 parameter is varied, (b) a_1 and (c) a_2 .
817 Vertical dotted lines show the optimal parameter values. 47

818 **Fig. 8.** Jensen-Shannon divergence as a function of σ the standard deviation of the AR1 process for
819 the cases $\phi = 0$ and $\phi = 0.984$. (a) $F = 7$, (b) $F = 18$ 48

820 **Fig. 9.** Scatterplots of the forcing as a function of the state variable given by the two-scale Lorenz
821 '96 model (gray dots) and the one given by the deterministic (a) and the stochastic parame-
822 terizations, $\phi = 0$ (b) and $\phi = 0.984$ (c), with optimal parameters (black dots) for the $F = 18$
823 case. 49

824 **Fig. 10.** Histogram PDFs for the nature integration with $F = 18$ (continuous line), for the imperfect
825 model with the deterministic parameterization using optimal parameter values (dashed line)
826 and for the imperfect model with the stochastic parameterization using $\phi = 0$ (dotted line)
827 and $\phi = 0.984$ (gray line). 50



828 FIG. 1. (a) Permutation entropy (\mathcal{H}), (b) permutation statistical complexity (\mathcal{C}), and (c) the causal entropy-
 829 complexity plane ($\mathcal{H} \times \mathcal{C}$) for two-scale Lorenz '96 integrations as a function of the forcing F with a resolution
 830 of $\delta F = 0.01$. Vertical dotted lines in (a) and (b) divide the four dynamical regimes found. The minimal and
 831 maximal complexity values, \mathcal{C}_{min} and \mathcal{C}_{max} as a function of permutation entropy are shown with black solid
 832 curves in panel (c). Regime (i) represents a dissipative system, (ii) quasi-periodic regime with high entropy,
 833 (iii) quasi-periodic with low entropy and (iv) chaotic regime. The transition points between the regions are not
 834 represented in panel (c) to improve visibility of the different regimes. The coupling factor in these experiments
 835 is $h = 1$.

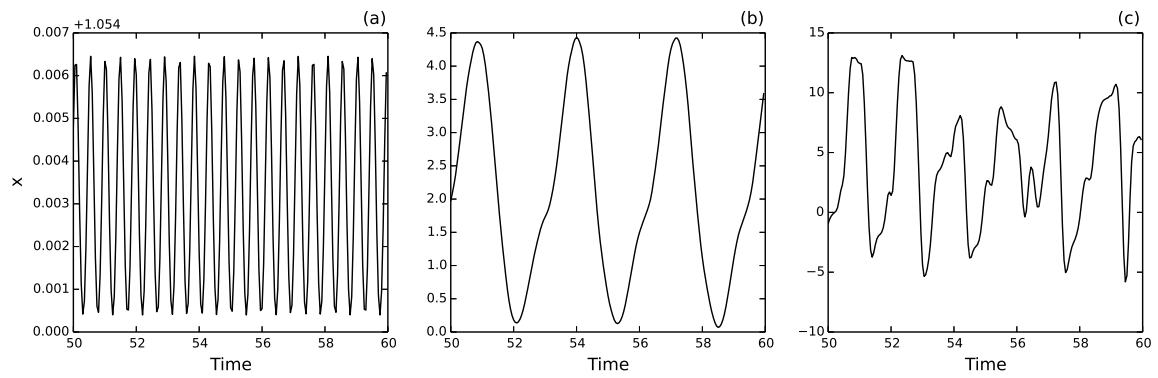
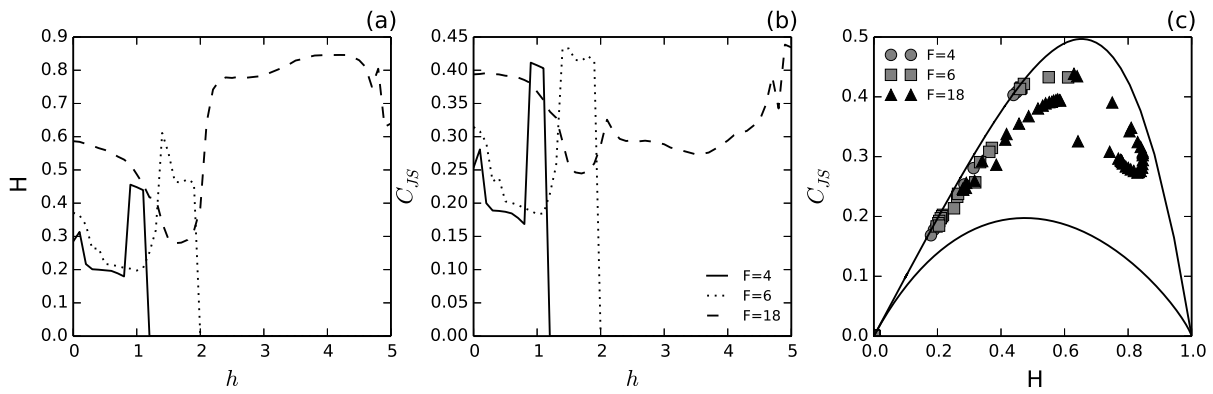
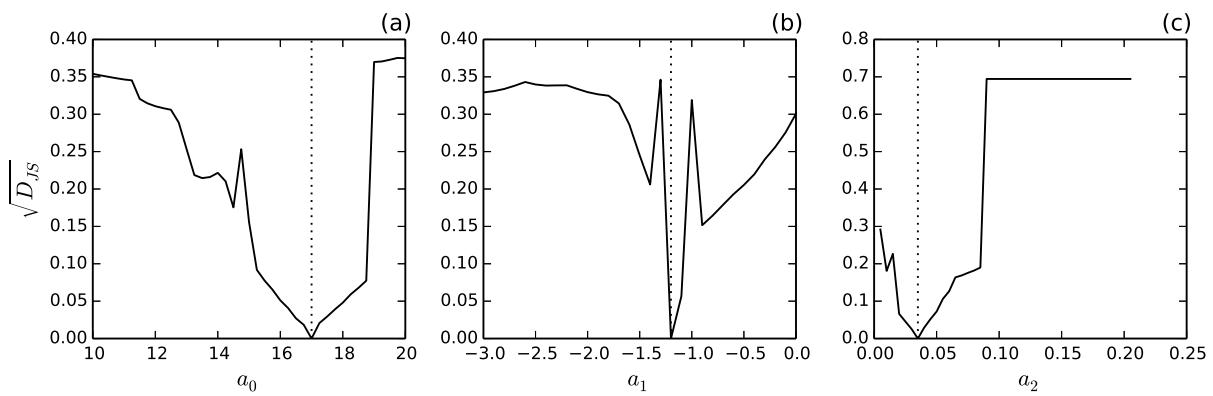


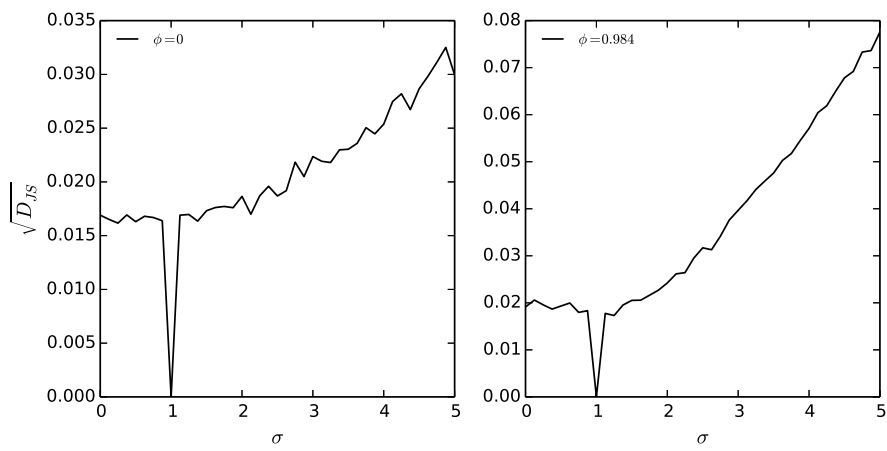
FIG. 2. Time series of a two-scale Lorenz '96 variable for (a) $F = 4$, (b) $F = 7$, and (c) $F = 18$.



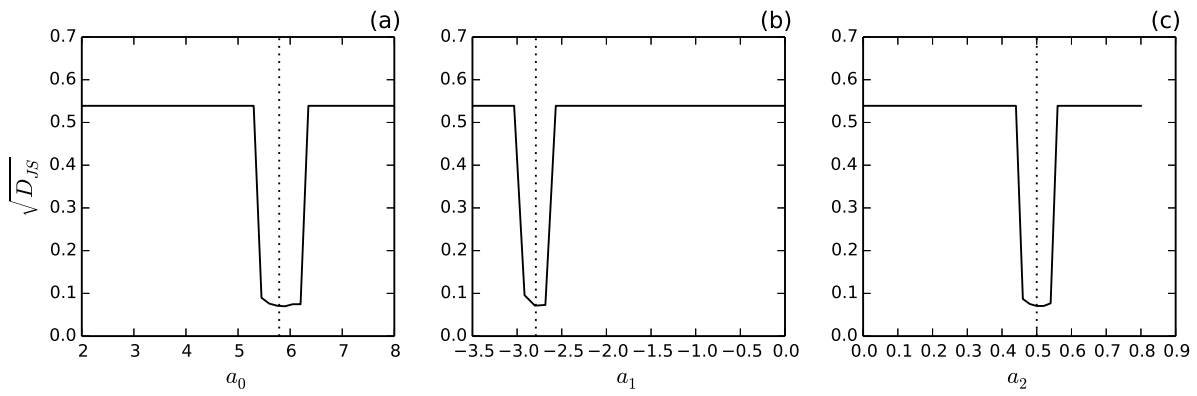
836 FIG. 3. (a) Permutation entropy (\mathcal{H}), (b) permutation statistical complexity (\mathcal{C}), and (c) the causal entropy-
 837 complexity plane ($\mathcal{H} \times \mathcal{C}$) for two-scale Lorenz '96 integrations with varying coupling constant h in steps of
 838 $\delta h = 0.1$ for $F = 4$ (continuous line, circle points), $F = 6$ (dotted curves, square points) and $F = 18$ (dashed
 839 curves, triangle points).



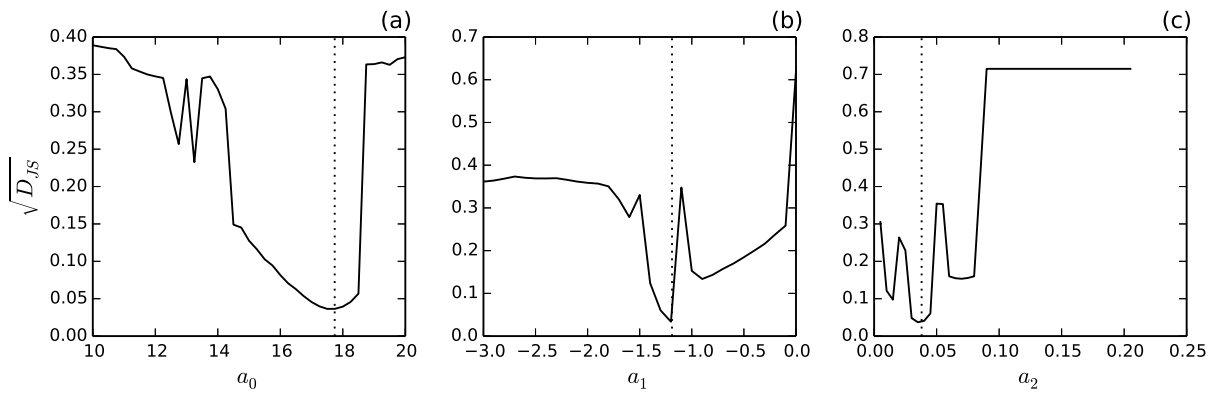
840 FIG. 4. Jensen-Shannon divergence as a function of a_0 , a_1 and a_2 under the perfect model assumption. The
 841 true parameter values are shown with vertical dotted lines. The square root of Jensen-Shannon divergence is
 842 used to make visible small values close to the minimum.



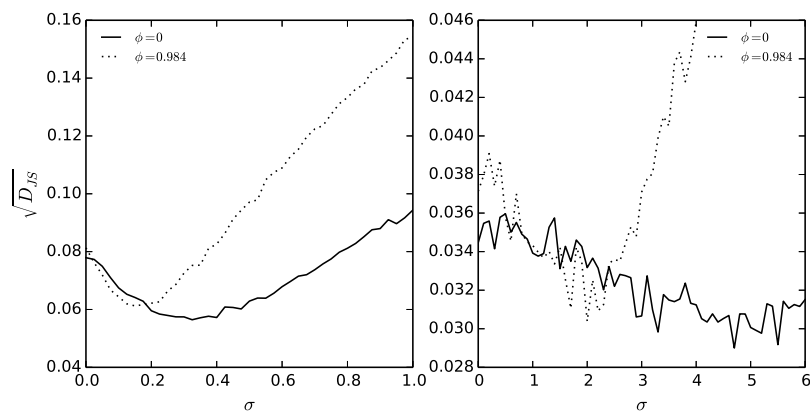
843 FIG. 5. Jensen-Shannon divergence as a function of the standard deviation, σ , and autoregressive parameter
 844 values (a) $\phi^t = 0$, and (b) $\phi^t = 0.984$ for the perfect model experiments. The other parameters are kept fixed at
 845 the optimal values.



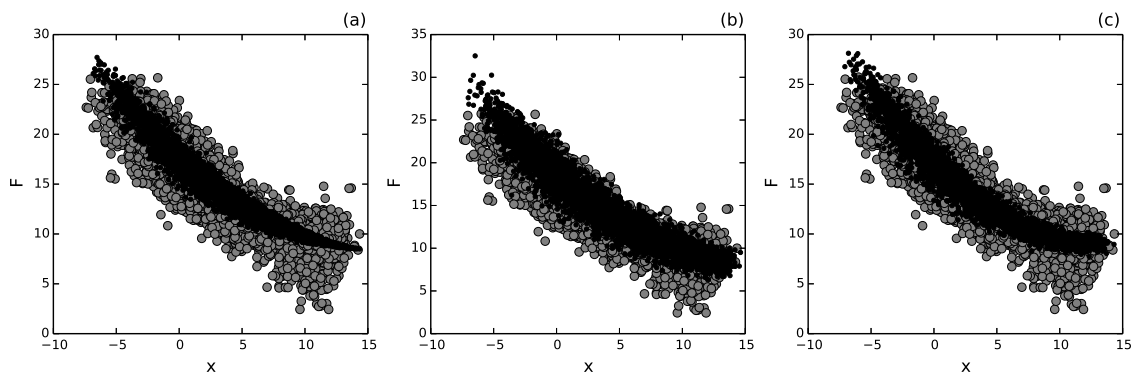
846 FIG. 6. Jensen-Shannon divergence between the probability distribution from the model integration with a
 847 given set of parameters, and the one from the natural two-scale Lorenz '96 system evolution for an external
 848 forcing of $F = 7$. Two parameters are kept fixed at the estimated values (Table 2) and the third one is varied: a)
 849 a_0 , b) a_1 , and c) a_2 dependencies. Vertical dotted lines show the optimal parameter values.



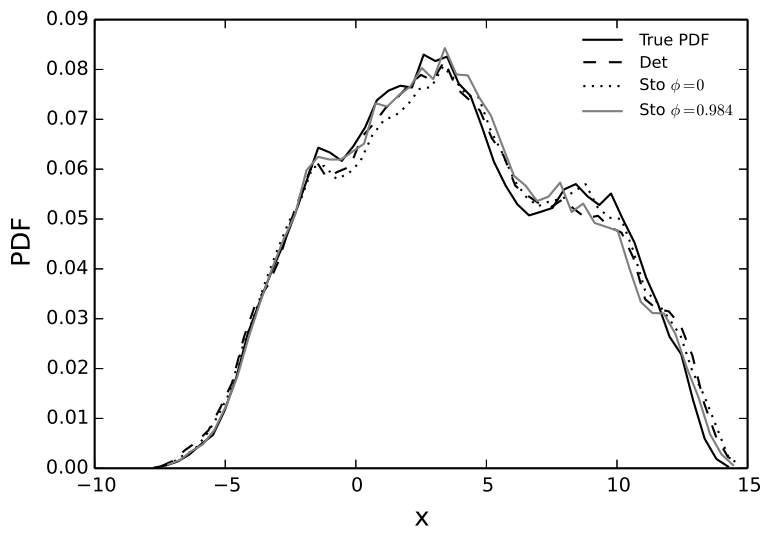
850 FIG. 7. Jensen-Shannon divergence between the probability distribution from the model integration with a
 851 given set of parameters, and the one from the natural two-scale Lorenz '96 system evolution for an external
 852 forcing of $F = 18$. One parameter value is varied and the other two are kept fixed at the optimal values (Table 2),
 853 (a) a_0 parameter is varied, (b) a_1 and (c) a_2 . Vertical dotted lines show the optimal parameter values.



854 FIG. 8. Jensen-Shannon divergence as a function of σ the standard deviation of the AR1 process for the cases
 855 $\phi = 0$ and $\phi = 0.984$. (a) $F = 7$, (b) $F = 18$.



856 FIG. 9. Scatterplots of the forcing as a function of the state variable given by the two-scale Lorenz '96
 857 model (gray dots) and the one given by the deterministic (a) and the stochastic parameterizations, $\phi = 0$ (b) and
 858 $\phi = 0.984$ (c), with optimal parameters (black dots) for the $F = 18$ case.



859 FIG. 10. Histogram PDFs for the nature integration with $F = 18$ (continuous line), for the imperfect model
 860 with the deterministic parameterization using optimal parameter values (dashed line) and for the imperfect model
 861 with the stochastic parameterization using $\phi = 0$ (dotted line) and $\phi = 0.984$ (gray line).